Critical cluster size of metallic Cr and Mo nanoclusters

S. H. Huh, H. K. Kim, J. W. Park, and G. H. Lee*
Department of Chemistry, College of Natural Sciences, Kyungpook National University, Taegu 702-701, South Korea
(Received 3 March 2000)

It is an intrinsic question whether or not the small metallic nanoclusters might have a structure different from the bulk structure. We observed a face-centered-cubic (fcc) structure for small Cr and Mo nanoclusters rather than a bulk body-centered-cubic (bcc) structure. We determined the critical cluster size n_{crit} to be 490 ± 100 for metallic Cr nanoclusters and the range of the n_{crit} to be 1460–3900 for metallic Mo nanoclusters at which a structural transition from the fcc structure into the bulk bcc structure occurred.

I. INTRODUCTION

Although the structural studies on metal clusters with the cluster size $n<10$ are numerous,[1] those on metallic nanoclusters with n between 10 and 10 000 are few. It is an intrinsic question whether or not the metal clusters will monotonically approach the bulk structure as n increases. However, the metal clusters carry a large surface energy because of a large surface-to-volume ratio and thus can have a structure different from the bulk structure in order to decrease a large surface energy.

Tománek, Mukherjee, and Bennemann had theoretically predicted that metal clusters with a bulk body-centered-cubic (bcc) structure would have a face-centered-cubic (fcc) structure when n is small.[2] In fact, we observed a structural evolution from amorphous→face-centered-cubic(fcc)→bulk body-centered-cubic(bcc) structures as n increased in the previous work on metallic W nanoclusters,[3] which proved the existence of the fcc structure predicted by Tománek, Mukherjee, and Bennemann.

In this work, we investigated the structural evolution of metallic Mo nanoclusters with increasing n. We observed that the structure evolved such that the amorphous→fcc→bcc structures as n increased, similar to metallic W nanoclusters. We determined the critical cluster size n_{crit} for both the Cr and Mo nanoclusters at which a structural transition from the fcc structure into the bulk bcc structure occurred. We discussed why the n_{crit} was in the order of $n_{crit}(\text{W clusters}) > n_{crit}(\text{Mo clusters}) > n_{crit}(\text{Cr clusters})$ for the group-VI transition-metal clusters.

II. EXPERIMENT

Metallic Cr and Mo nanoclusters were produced by using the thermal decomposition method that had been previously described in detail.[4] This method combines thermal decomposition of the metal carbonyl $M(CO)_6$ (M=Cr and Mo) vapor by using a resistively heated filament with collision-induced clustering between the decomposed neutral metal M atoms. The reaction begins with a hot filament, which decomposes the $M(CO)_6$ vapor into the neutral M atoms and the CO's, and then subsequent collisions between the decomposed neutral metal atoms lead to the metallic nanoclusters. In this method, the nichrome (Ni/Cr/Fe alloy) wire was used as a filament. However, any kind of resistive material can be used as a filament. The filament was heated by flowing alternating current (ac) through the filament.

A certain amount of metal carbonyl sample that corresponded to a certain vapor pressure was weighed and then loaded into the reaction chamber. The reaction chamber was heated up to 150 °C or so in order to vaporize the metal carbonyl sample, which in turn became decomposed into the metal atoms and the CO's by the hot filament as described previously. The final products were the black and metallic nanoclusters with a narrow size distribution and with a purity of more than 95% determined by the inductively coupled plasma atomic emission spectrometer. The usual production condition included the 10–100 Torr $Mo(CO)_6$ vapor, the 0–10-atm rare gas He or Ar, and the filament voltage, which corresponded to the filament temperature[5] of 300–400 °C.

The cluster size could be generally controlled by diluting the metal carbonyl vapor with a high pressure of He or Ar gas even though the size control was difficult in case of Cr clusters. By increasing the rare-gas pressure, the cluster size was generally decreased.

After the nanoclusters were produced, the reaction chamber was pumped out to eliminate the toxic CO's remaining in the reaction chamber. Then the nanoclusters were exposed to air for collection for further experiments such as structural analysis by using x-ray diffraction (XRD) apparatus, size analysis by using a transmission electron microscope (TEM), and purity analysis by using the inductively coupled plasma atomic emission spectrometer.

The high purity of metallic nanoclusters indicates that the CO's hardly contaminated the metal clusters during the cluster formation reaction under the experimental condition used in the present experiment. It might be expected that there could be some physisorption of the CO's on metal cluster surfaces during cluster formation. However, the cluster temperature was likely to be close to the filament temperature (i.e., 300–400 °C) because metallic nanoclusters were formed close to the filament environment, and thus the CO's should be desorbed immediately. Furthermore, it is highly unlikely that the CO's were chemisorbed onto the metal cluster surface during cluster formation. If the CO's were chemisorbed, a large amount of contamination by CO's and their dissociation products such as carbons and oxygens should have severely degraded the purity of metal clusters, which, however, has never been observed. The XRD patterns have never showed any indication of peaks either from metal car-

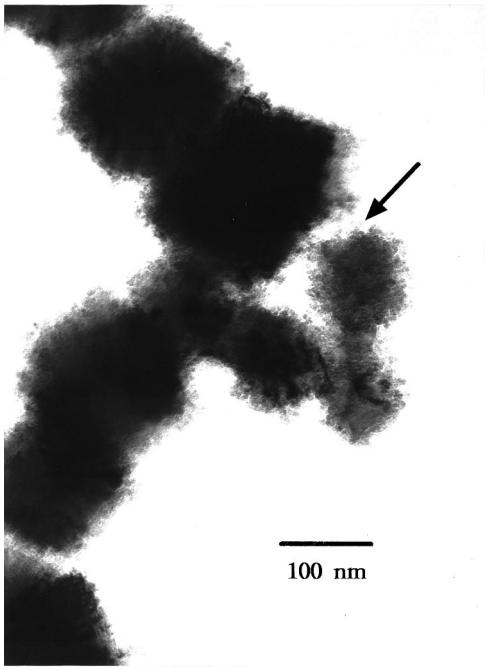

FIG. 1. The TEM micrograph of metallic Cr nanoclusters in aggregated form. The arrow indicates one of the areas in which the individual Cr nanoclusters can be observed.

bides or from metal oxides. The remaining tiny impurities, less than 5%, mostly likely came from oxygens and water molecules absorbed by metal clusters during exposure to air. There was, however, no change in purity, XRD pattern, and TEM micrograph with time after exposure to air at least for a few days, which indicates that metallic Cr and Mo nanoclusters were almost inert to air.

III. RESULTS AND DISCUSSION

A. Cr nanoclusters

Figure 1 represents the TEM micrograph of metallic Cr nanoclusters. As can be seen in Fig. 1, the individual Cr clusters with a narrow size distribution were aggregated into a cubic form. Edelstein *et al.* also observed a similar aggregation in the Mo metal particles produced by using the Ar-ion sputtering method.[6] Thus, the aggregation of the metal clusters is likely a general phenomenon when there exists a high density of metal clusters. Figure 2 represents the cluster-diameter histogram obtained by using cluster diameters observed in the TEM micrograph. As can be seen in Fig. 2, the cluster-diameter distribution was very narrow and had a tail toward larger diameters. The tail in the cluster-diameter distribution is typical for all metal clusters[7–9] and represents a characteristic log-normal distribution.[7] Figure 3 shows the log-normal distribution function fit of the data. The average cluster diameter was determined to be 2.62 ± 0.02 nm.

Figure 4(a) represents the XRD pattern of metallic Cr nanoclusters. As can be seen in Fig. 4(a), the XRD pattern is a typical XRD pattern of the fcc substance except for the abnormal intensities of the second and third peaks. The enhanced intensities of these two peaks were due to the overlaps of the two bcc and fcc peaks assigned as

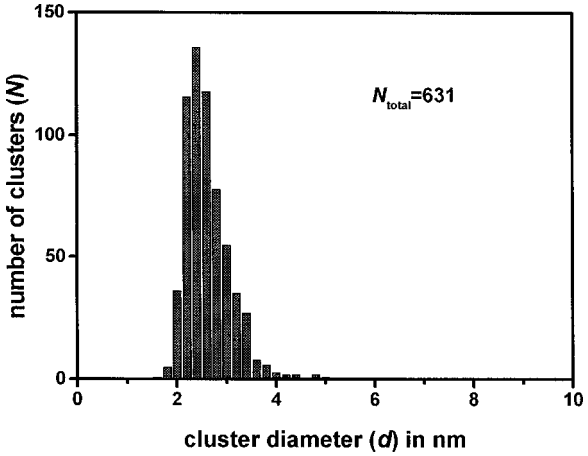

FIG. 2. Cluster diameter histogram of metallic Cr nanoclusters. The total number (N_{total}) of clusters used in the histogram was 631.

bcc(110)+fcc(200) and bcc(200)+fcc(220) on top of the corresponding peaks, respectively. The peaks were fitted to the Lorentzian function to obtain the cell constants and the bond lengths as provided in Table I.[10] In order to make sure that the fcc Cr clusters were not metastable, we took the XRD pattern after we slowly annealed the Cr clusters up to 500 °C as represented in Fig. 4(b). Apparently, there is no change in the XRD pattern, which implies that the fcc structure was due to the small cluster size.

We estimated the ratio in the amount of the bcc clusters to that of the fcc clusters. First, we generated the theoretical XRD patterns of both the bcc and fcc clusters by calculating the peak intensities[11] and by using the observed full width at half maximum values (FWHM's) of the peaks and the peak positions (2θ). They are represented in Figs. 5(a) and 5(b), respectively. Then, we added the two theoretical XRD patterns after we weighted the peak intensities with the ratio of the amount of the bcc clusters to that of the fcc clusters. We repeated the weighting procedure until we reproduced the observed XRD pattern. In weighting the XRD patterns, we used the fact that the ratio in the intensity of the bcc (110) peak to that of the fcc (200) peak should be 1:2 when equal

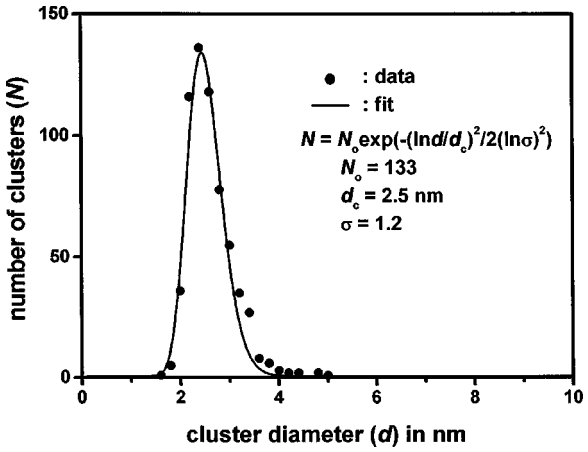

FIG. 3. The log-normal distribution function fit to the cluster diameter histogram. The d_c and the σ indicate the most probable cluster diameter and the standard deviation, respectively. The average cluster diameter ($\overline{d}$) was estimated to be 2.62 ± 0.02 nm.

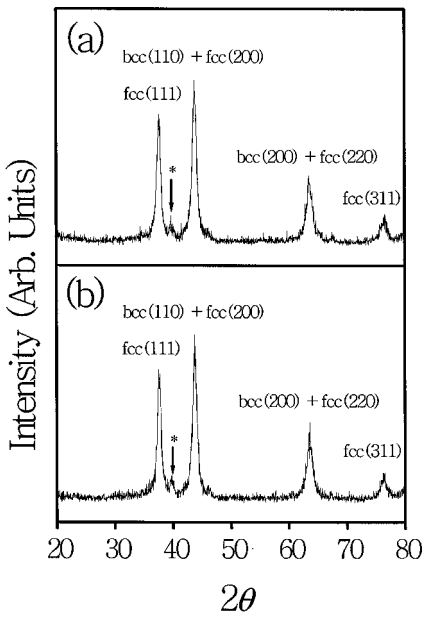

FIG. 4. (a) The XRD pattern of metallic Cr nanoclusters on the Pt substrate. (b) The XRD pattern of the annealed Cr nanoclusters up to 500 °C on the Pt substrate. The asterisk indicates the Pt (111) peak. The indices are the Miller indices (*hkl*).

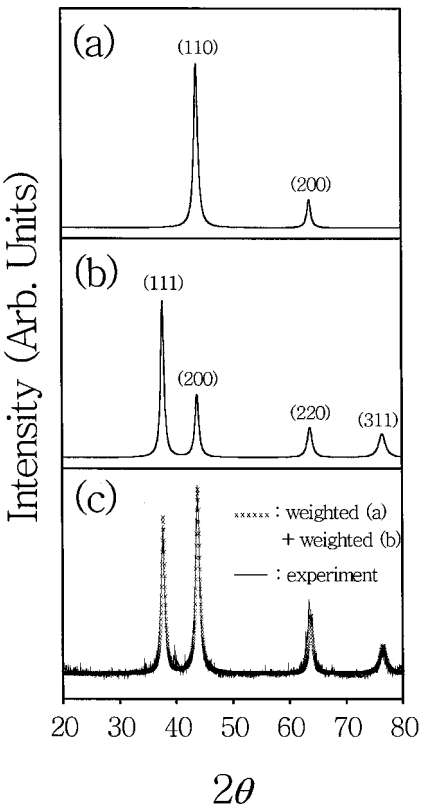

FIG. 5. (a) The theoretical XRD pattern of the bcc Cr nanoclusters. (b) The theoretical XRD pattern of the fcc Cr nanoclusters. (c) The combined XRD pattern of the weighted XRD pattern (a) + the weighted XRD pattern (b) and the observed XRD pattern already presented in Fig. 4(a) for comparison.

amounts of the bcc and fcc Cr clusters exist. We finally reproduced the observed XRD pattern as presented in Fig. 5(c) by using the ratio of 79 (the bcc clusters): 21 (the fcc clusters).

Cluster size (n) can be calculated by using a simple equation $n_i \cong (R/r_i)^3 f_i$ in which i indicates the cluster structure, i.e., fcc or bcc, n_i is the cluster size, R is the cluster radius, r_i is the atomic radius, and f_i is the packing fraction ($=0.68$ for the bcc structure and 0.74 for the fcc structure).[12] In the above equation, r_i is obtained from the cell constant as provided in Table I. Since the r_i and f are constants, the reliability of n depends on R. In order to determine n_{crit}, the critical cluster diameter (d_{crit}) should be determined, from which the critical cluster radius (R_{crit}) is obtained by using $R_{\mathrm{crit}} = d_{\mathrm{crit}}/2$. Since the above estimated ratio in the amount of fcc clusters to that of bcc clusters is not much different from 50:50, d_{crit} is likely close to the average cluster diameter of 2.62 ± 0.02 nm obtained from the cluster-diameter distribution in Fig. 3. Also, d_{crit} is likely close to the cluster diameter, which gives the first 21% of the total area in Fig. 3 for the fcc clusters and the remaining 79% for the bcc clusters. Since we know that the cluster structure evolves from the fcc structure into the bcc structure from the previous[3] and present works, the first 21% area corresponds to the fcc clusters and the remaining 79% area corresponds to the bcc clusters. From Fig. 3, the cluster diameter that gives the above area ratio was determined to be 2.14 ± 0.02 nm. Thus, taking average value from these two cluster diameters for d_{crit}, the average $R_{\mathrm{crit}} = (2.62 + 2.14)/4 = 1.19 \pm 0.02$ nm. Thus, by using a simple equation $n \cong (R/r)^3 f$ given above and taking the $n_{\mathrm{crit}} = [(n_{\mathrm{crit}})_{\mathrm{fcc}} + (n_{\mathrm{crit}})_{\mathrm{bcc}}]/2$, we found n_{crit} to be 490. The error in the n_{crit} mostly results from the error in the R and the

TABLE I. The cell constant (a), the atomic radius (r), the bond length ($2r$) between the nearest atoms, and the bond-length difference ($\Delta 2r = 2r_{\mathrm{fcc}} - 2r_{\mathrm{bcc}}$) in nanometers for the group-VI transition-metal clusters.

Cluster	Structure	a	r	$2r$	$\Delta 2r$	Reference
Cr	fcc	0.413	0.146	0.292	0.040	This work
	bcc	0.292	0.126	0.252		This work
		0.289	0.125	0.250		15 (bulk value)
Mo	fcc	0.419	0.148	0.296	0.024	This work; 12
	bcc	0.315	0.136	0.272		This work
		0.315	0.136	0.272		15 (bulk value)
W	fcc	0.416	0.147	0.294	0.020	16
	bcc	0.317	0.137	0.274		16
		0.317	0.137	0.274		15 (bulk value)

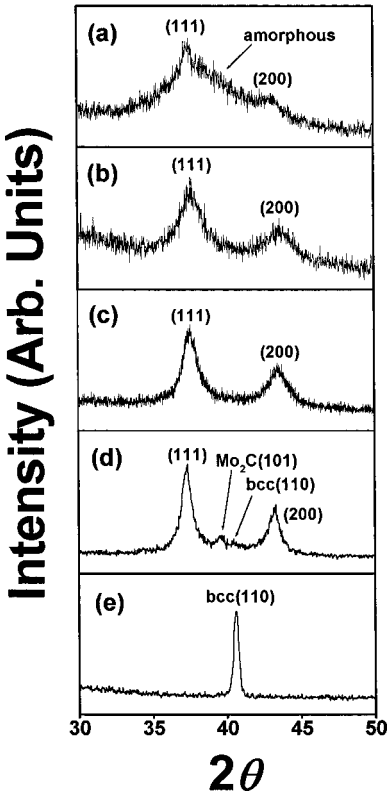

FIG. 6. (a) The XRD pattern of metallic Mo nanoclusters produced by decomposing the 30-Torr $Mo(CO)_6$ diluted by the 10-atm He gas. (b) The XRD pattern of metallic Mo nanoclusters produced by decomposing the 30-Torr $Mo(CO)_6$ diluted by the 10-atm Ar gas. (c) The XRD pattern of metallic Mo nanoclusters produced by decomposing the 30-Torr $Mo(CO)_6$ diluted by the 4-atm Ar gas. (d) The XRD pattern of metallic Mo nanoclusters produced by rapidly decomposing 30-Torr $Mo(CO)_6$ by using a high filament voltage of 20 V ac, which corresponded to the filament temperature of ~650 °C. (e) The XRD pattern of metallic Mo nanoclusters prepared by melting the above (b) clusters by heating them up to the melting point of ~800 °C for 2 h and then by slowly cooling them down to the room temperature.

error in the R is mostly the range from the average R_{crit}. Taking into account this range, the error in the n_{crit} is 100.

B. Mo nanoclusters

Figures 6(a)–6(e) represent the XRD patterns of metallic Mo nanoclusters prepared at different cluster sizes. The cluster size increases from (a) to (e), which can be noticed from the decrease of the FWHM of the peaks from (a) to (e).[3,13] The XRD pattern in Fig. 6(a) consists of the amorphous and fcc peaks, from which we can notice that the fcc clusters begin to appear. The XRD patterns in Figs. 6(b) and 6(c) only consist of the fcc structure. The XRD pattern in Fig. 6(d) consists of the fcc and bulk bcc structures with an additional tiny hexagonal α-$Mo_2C(101)$ peak, from which we can notice that the bcc clusters begin to appear. The clusters in Fig. 6(d) were produced by rapidly decomposing the 30-Torr $Mo(CO)_6$ vapor by using a high filament voltage of 20 V ac, which corresponded to the filament temperature of ~650 °C at which a small amount of α-Mo_2C particles were also produced, similar to the previous experiment on metallic

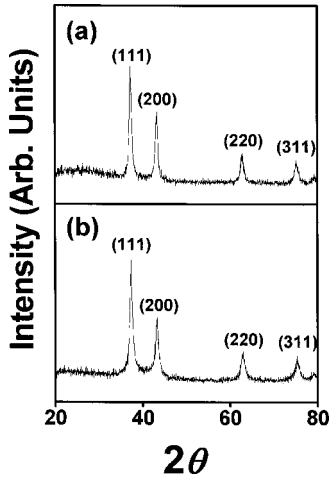

FIG. 7. (a) The XRD pattern of metallic Mo nanoclusters at room temperature. (b) The XRD pattern of metallic Mo nanoclusters after being annealed up to 700 °C for 2 h.

W nanoclusters.[3] Finally, the XRD pattern in Fig. 6(e) only consists of the bulk bcc structure, which was obtained by heating the above (b) clusters up to the melting point of ~800 °C. The peaks were fitted to the Lorentzian function to obtain the cell constants and the bond lengths as provided in Table I.[14]

In order to make sure that the fcc Mo nanoclusters were not metastable as done in metallic Cr nanoclusters, we took the XRD pattern after we annealed the fcc Mo clusters up to 700 °C for 2 h. However, there was no change in the XRD pattern as represented in Fig. 7(b), which indicates that the fcc structure was due to the small cluster size. Thus, the XRD patterns presented in Figs. 6(a)–6(e) indicate that the cluster structure changed from amorphous→fcc→bulk bcc as cluster size increased.

In order to determine the critical cluster size n_{crit}, we used the XRD pattern in Fig. 6(d), which showed both bcc and fcc peaks. As done in metallic Cr nanoclusters, the n_{crit} can be determined from the cluster-diameter distribution. However, one problem in metallic Mo nanoclusters is that the ratio of the amount of fcc clusters to that of bcc clusters could not be accurately determined because the bcc (110) peak in Fig. 6(d) was not well resolved from the hexagonal α-$Mo_2C(101)$ peak. That is, the peak intensity of the bcc (110) peak could not be accurately measured, and thus the accurate ratio in the peak intensity could not be estimated. As a result, the ratio in the amount of fcc clusters to that of bcc clusters could not be accurately determined. Thus, we just roughly estimated the range of the n_{crit} as follows. Figure 8 represents the cluster-diameter histogram obtained from the TEM micrograph, representing a characteristic log-normal distribution.[7] The distribution looks wider than that of Cr nanoclusters. This is because Mo nanoclusters in Fig. 6(b) were produced under somewhat dramatic conditions in which the α-Mo_2C particles were also produced, as described previously. Figure 9 shows the log-normal distribution function fit of the data. The average cluster diameter was determined to be 2.4 nm from the fit. Here, the strong intensities of the fcc clusters in the XRD pattern of Fig. 6(d) are likely from the Mo nanoclusters with diameter around 2.40 $\pm$0.02 nm, whereas the weak intensity of the bcc clusters is

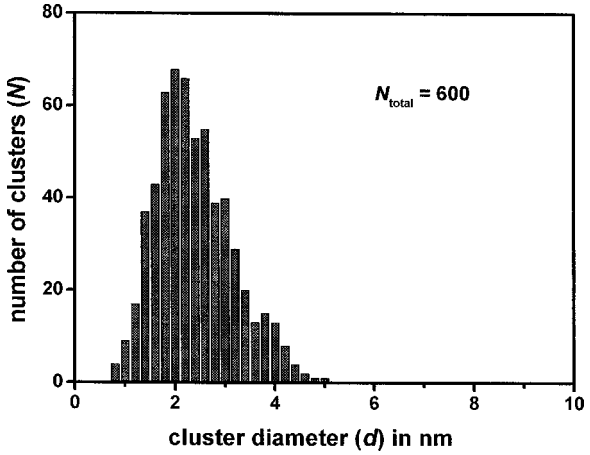

FIG. 8. Cluster diameter histogram of metallic Mo nanoclusters represented in the XRD pattern of Fig. 6(d). The total number (N_{total}) of clusters used in the histogram was 600.

likely from the Mo nanoclusters in the tail region. In order to estimate the range of the cluster diameters in the tail region that corresponded to the bcc clusters, we estimated the ratio in the intensities of the fcc (200) peak to the bcc (110) peak in Fig. 6(d) to be roughly 94:6 by fitting the peaks to the Lorentzian function. Then, we estimated the ratio in the amounts of fcc clusters to bcc clusters to be 88:12 by noting that when equal amounts of fcc clusters and bcc clusters exist, the intensity ratio of the fcc (200) peak to the bcc (110) peak should be 2:1 as done in Cr nanoclusters. Thus, the cluster-diameter range, which gave 12% of the total area in Fig. 9, was 3.6–5.0 nm. By using the same equation and method as used for the Cr nanoclusters, the use of d of 3.6–5.0 nm for the tail region provided the range for n_{crit} of 1460–3900.

Scherrer's formula can be also used to roughly determine the cluster diameter[3,13] and thus the cluster size. In Scherrer's formula, the FWHM's of the peaks in the XRD pattern are used to estimate the cluster diameters.[3,13] As done in the previous work on metallic W nanoclusters,[3] the upper bound of the n_{crit} can be estimated by using the FWHM's of the bcc

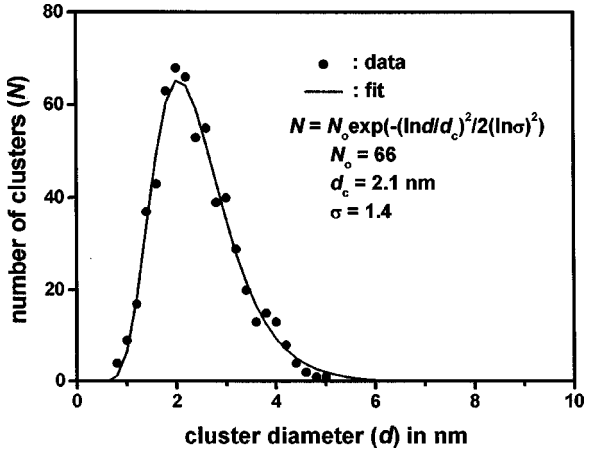

FIG. 9. The log-normal distribution function fit to the cluster diameter histogram. The d_c and the σ indicate the most probable cluster diameter and the standard deviation, respectively. The average cluster diameter ($\overline{d}$) was estimated to be 2.40 ± 0.02 nm.

TABLE II. The critical cluster size n_{crit} determined from the present and previous works and the theoretical values.

Cluster	n_{crit}	Reference
Cr	490 ± 100	This work
	580	2
Mo	1460–3900	This work
	2630	2
W	7200–10 470	3
	5660	2

peaks when the small but well-resolved bcc peaks begin to appear in the XRD pattern, whereas the lower bound of the n_{crit} can be estimated by using the FWHM's of the fcc peaks in the same XRD pattern. However, the bcc (110) peak in the XRD pattern of Fig. 6(d) was not resolved from the hexagonal α-Mo_2C(101) peak so that the reliable FWHM and eventually the upper bound n_{crit} from it could not be estimated. The lower bound of the n_{crit} estimated by using the FWHM (i.e., 1.0°) of the fcc (111) peak in Fig. 6(d) is 3160, which is within the above range. From these two calculations, it is likely that the n_{crit} of the metallic Mo nanoclusters is expected to be within the above range.

Compared to the theoretical prediction by Tománek, Mukherjee, and Bennemann,[2] our experimental work is generally consistent with it. First, we observed the fcc structure when cluster size was small, as predicted by theory. Second, the estimated n_{crit} is somewhat close to the theoretically predicted values.

C. Why is n_{crit}(W clusters) > n_{crit}(Mo clusters) > n_{crit}(Cr clusters)?

Table II summarizes the n_{crit}'s determined from the present and previous works. As provided in Table II, the order in the n_{crit} is $n_{\text{crit}}(\text{W clusters}) > n_{\text{crit}}(\text{Mo clusters}) > n_{\text{crit}}(\text{Cr clusters})$. We could explain the above observation by using the bond lengths obtained from the XRD data. From Table I, two important observations on the bond length can be noticed: (1) the bond length ($2r$) of the fcc structure is greater than the $2r$ of the bulk bcc structure for all metal clusters and (2) the bond-length difference ($\Delta 2r = 2r_{\text{fcc}} - 2r_{\text{bcc}}$) is $\Delta 2r(\text{Cr clusters}) > \Delta 2r(\text{Mo clusters}) > \Delta 2r(\text{W clusters})$. The first observation explains why the structure changes from the fcc structure into the bulk bcc structure as cluster size increases, and the second observation explains why $n_{\text{crit}}(\text{W clusters}) > n_{\text{crit}}(\text{Mo clusters}) > n_{\text{crit}}(\text{Cr clusters})$.

First, the larger $2r$ of the fcc structure than that of the bcc structure for all metal clusters is due to the larger coordination number of the fcc structure (= 12) than the bcc structure (= 8).[17] Since $2r$ of the fcc structure is larger than that of the bcc structure, the bonding of the fcc structure is weaker than that of the bcc structure. However, since the fcc structure provides the nanoclusters with a lower surface energy (eventually a lower cluster energy) due to a lower surface to volume ratio than the bcc structure,[2,18] the small nanoclusters have the fcc structure rather than the bulk bcc structure, as observed. However, as cluster size increases, the surface-to-volume ratio becomes negligible, and thus the surface-

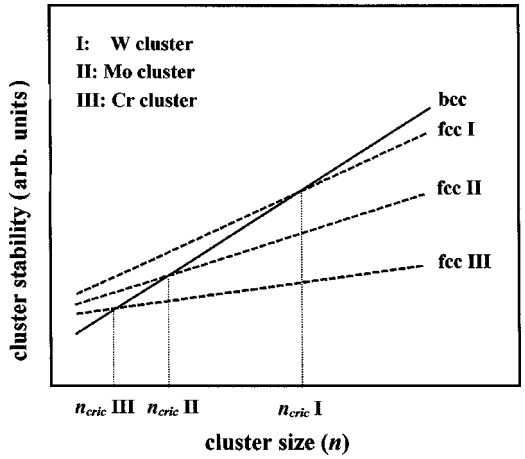

FIG. 10. The qualitative graphical presentation for the explanation of the $n_{\mathrm{crit}}(\mathrm{W\ clusters}) > n_{\mathrm{crit}}(\mathrm{Mo\ clusters}) > n_{\mathrm{crit}}(\mathrm{Cr\ clusters})$. The stability curve of the bcc structure was chosen to be the common for all metal clusters for convenience sake although each metal cluster has its own curve.

energy contribution to cluster energy will be negligible. Finally, the clusters will have the bulk bcc structure in order to minimize the cluster energy through the energy gain obtained from the stronger bonding of the bcc structure. This is the reason that the group-VI transition-metal clusters change their structure from the fcc structure into the bulk bcc structure as cluster size increases.

Second, the observed trend in the $\Delta 2r$ is due to the fact that the heavy atom has more extra electrons for bonding than the light atom, and thus the heavy-atom cluster can better deal with the coordination number increase than the light-atom cluster. Thus, the bond length of the fcc structure did not much change from that of the bcc structure in case of heavy-atom clusters. This implies (i) that the stability of the fcc structure with respect to that of the bcc structure when $n \ll n_{\mathrm{crit}}$ is better for the clusters with smaller $\Delta 2r$ than those with the larger $\Delta 2r$ and (ii) that the stability increase of the fcc structure with n (i.e., the slope of the fcc structure in Fig. 10) is larger for clusters with smaller $\Delta 2r$ than those with larger $\Delta 2r$. As a result, the crossing between the fcc and bcc curves in Fig. 10 will occur at larger n for the clusters with smaller $\Delta 2r$ than those with larger $\Delta 2r$. Thus, the larger n_{crit} occurs in clusters with smaller $\Delta 2r$. A combined graphical explanation of these statements (i) and (ii) is given in Fig. 10. Thus, the n_{crit} will be such that $n_{\mathrm{crit}}(\mathrm{W\ clusters}) > n_{\mathrm{crit}}(\mathrm{Mo\ clusters}) > n_{\mathrm{crit}}(\mathrm{Cr\ clusters})$, which is consistent with the theoretical prediction.[2]

IV. CONCLUSION

We can answer the question why the small group-VI nanoclusters possessed fcc structure rather than bulk bcc structure when cluster size was small by considering the cluster energy because the cluster structure is determined by the cluster energy. For small clusters, the surface-to-volume ratio is so huge that the surface energy plays the critical role in determining the cluster energy. Note that the fcc structure is more compact than the bcc structure and thus provides a smaller number of surface atoms than the bcc structure. As a result, the fcc structure provides a lower surface energy (eventually a lower cluster energy) than the bcc structure. This is the reason why small clusters have fcc structure rather than bulk bcc structure. We observed that the bond length of the fcc structure was longer than that of the bcc structure. Thus, the bonding of the fcc structure was weaker than that of the bulk bcc structure. However, the fcc structure of the small nanoclusters proves that the surface energy of the small clusters is very important in the cluster energy. However, as cluster size increases, the surface-to-volume ratio decreases (and eventually becomes negligible when the cluster size approaches the bulk limit). In these circumstances, the surface-energy effect on the cluster energy is negligible, and thus the clusters will have bulk bcc structure in order to have a lower cluster energy through the energy gain obtained from the stronger bonding of the bcc structure.

ACKNOWLEDGMENTS

This work was supported by the KOSEF and KRF. We thank the Korea Basic Science Institute for allowing us to use the x-ray diffraction apparatus, the transmission electron microscope, and the inductively coupled plasma atomic emission spectrometer. We also thank Professor Kit Bowen at Johns Hopkins University and Professor Y. H. Lee at Cheonpook National University for insightful discussions.

*Author to whom correspondence should be addressed. FAX: 82-53-950-5340. e-mail: ghlee@bh.kyungpook.ac.kr

[1] R. Kishi, H. Kawamata, Y. Negishi, S. Iwata, A. Nakajima, and K. Kaya, J. Chem. Phys. **107**, 10 029 (1997); M. Iseda, T. Nishio, S. Y. Han, H. Yoshida, A. Terasaki, and T. Kondow, *ibid.* **106**, 2182 (1997); V. Bonačić-Koutecký, J. Pittner, C. Fuchs, P. Fantucci, M. F. Guest, and J. Koutecký, *ibid.* **104**, 1427 (1996); C. Yannouleas, E. Vigezzi, and R. A. Broglia, Phys. Rev. B **47**, 9849 (1993); C. Wang, S. Pollack, T. Dahlseid, G. M. Koretsky, and M. M. Kappes, J. Chem. Phys. **96**, 7931 (1992); C. Gatti, S. Polezzo, and P. Fantucci, Chem. Phys. Lett. **175**, 645 (1990); D. M. Lindsay, Y. Wang, and T. F. George, J. Chem. Phys. **86**, 3500 (1987); W. Ekardt, Z. Penzar, and M. Sunjic, Phys. Rev. B **33**, 3702 (1986).

[2] D. Tománek, S. Mukherjee, and K. H. Bennemann, Phys. Rev. B **28**, 665 (1983).

[3] S. J. Oh, S. H. Huh, H. K. Kim, J. W. Park, and G. H. Lee, J. Chem. Phys. **111**, 7402 (1999).

[4] S. H. Huh, S. J. Oh, Y. N. Kim, and G. H. Lee, Rev. Sci. Instrum. **70**, 4366 (1999).

[5] The filament temperature was obtained from the technical data provided by the Pelican Wire Company, Inc., 6266 Taylor Road, Naples, FL 34109-1896.

[6] A. S. Edelstein, G. M. Chow, E. I. Altman, R. J. Colton, and D. M. Hwang, Science **251**, 1590 (1991).

[7] C. G. Granqvist and R. A. Buhrman, J. Appl. Phys. **47**, 2200 (1976).

[8] S. W. Han, Y. Kim, and K. Kim, J. Colloid Interface Sci. **208**, 272 (1998).

[9] K. M. McHugh, H. W. Sarkas, J. G. Eaton, C. R. Westgate, and

K. H. Bowen, Z. Phys. D: At., Mol. Clusters **12**, 3 (1989).

[10] XRD data of metallic Cr nanoclusters obtained by the fitting the XRD pattern in Fig. 4(a) to the Lorentzian function are {structure (hkl), 2θ, peak area} = {fcc (111), 37.52°, 190}, {bcc (110) + fcc(200), 43.83°, 252}, {bcc(200) + fcc(220), 63.46°, 128}, {fcc(311), 76.25°, 53}. The x-ray wavelength used was 0.1542 nm.

[11] B. D. Cullity, *Elements of X-ray Diffraction* (Addison-Wesley, Reading, MA, 1978), p. 139. The calculated peak intensities are 146 303 (110) and 21 460 (200) for the bcc structure; 615 242 (111), 292 605 (200), 171 679 (220), and 197 146 (311) for the fcc structure.

[12] G. H. Lee, S. H. Huh, and H. I. Jung, J. Mol. Struct. **440**, 141 (1998).

[13] B. D. Cullity, *Elements of X-ray Diffraction* (Ref. 11), Reading, MA, p. 102.

[14] The XRD data of metallic Mo nanoclusters obtained by the fitting the XRD patterns to Lorentzian function are $(hkl, 2\theta)$ = (111, 37.28°) and (200, 43.18°) for the fcc structure and (110, 40.52°) for the bcc structure. The x-ray wavelength used was 0.1542 nm.

[15] P. Villars and L. D. Calvert, *Pearson's Handbook of Crystallographic Data for Intermetallic Phases* (American Society for Metals, Metals Park, OH, 1989), Vol. 2.

[16] See Ref. 3. The XRD data of metallic W nanoclusters obtained by the fitting the XRD patterns to the Lorentzian function are the $(hkl, 2\theta)$ = (111, 37.48°), (200, 43.51°), (220, 62.32°), and (311, 75.82°) for the fcc structure and (110, 40.34°) and (211, 73.22°) for the bcc structure. The x-ray wavelength used was 0.1542 nm.

[17] L. Pauling, *The Nature of the Chemical Bond*, 3rd ed. (Cornell University Press, New York, 1995), p. 413.

[18] At $n_{fcc} = n_{bcc}$, the number of the surface atoms of the fcc structure (N_{fcc}) divided by that of the bcc structure $(N_{bcc}) \cong (f_{bcc}/f_{fcc})^{2/3} = (0.68/0.74)^{2/3} = 0.95$ by assuming a spherical shape of the cluster, by using $n \cong (R/r)^3 f$ (see text), and by using $N \cong$ (surface area)/(atomic area).